Article

Hyperelastic Material Parameter Determination and Numerical Study of TPU and PDMS Dampers

Carina Emminger [1,*], Umut D. Cakmak [1,*], Rene Preuer [2], Ingrid Graz [2] and Zoltan Major [1]

[1] Christian Doppler Laboratory for Soft Structures for Vibration Isolation and Impact Protection (ADAPT), Institute of Polymer Product Engineering, Johannes Kepler University Linz, Altenbergerstrasse 69, 4040 Linz, Austria;
carina.emminger@jku.at, umut.cakmak@jku.at, zoltan.major@jku.at

[2] Christian Doppler Laboratory for Soft Structures for Vibration Isolation and Impact Protection (ADAPT), School of Education, STEM Education, Johannes Kepler University Linz, Altenbergerstrasse 69, 4040 Linz, Austria,
ingrid.graz@jku.at, rene.preuer@jku.at

* Correspondence: carina.emminger@jku.at, umut.cakmak@jku.at

Abstract: Dampers provide safety by control of unwanted motion, due to conversion of mechanical work into another form of energy (e.g., heat). State of the art materials are elastomers including thermoplastic-elastomers. For polymer-appropriate replacement of multi-component shock absorbers comprising mounts, rods, hydraulic fluids, pneumatic devices, or electro-magnetic devices, among others, deep insights of the dynamic thermo-mechanical characteristics of damper materials have to be gained. The ultimate objective is to reduce complexity by utilizing inherent material damping rather than structural (multi-component) damping properties. The objective of this work was to compare the damping behavior of different elastomeric materials including thermoplastic poly(urethane) (TPU), and silicone rubber blends (mixtures of different poly(dimethylsiloxane) (PDMS)). Therefore, the materials were hyper- and viscoelastic characterized, a finite element calculation of a ball-drop test was performed, and for validation the rebound resilience was measured experimentally. In an attempt, the coil-over shock absorber of a model car was replaced by a damper made of the examined and modeled materials. The results revealed that the material parameter determination methodology is reliable, and the data applied for simulation lead to realistic predictions. Interestingly, the rebound resilience of the mixture of soft and hard PDMS (50:50)w% is the highest and the lowest values were measured for TPU.

Keywords: hyperelastic material modelling, material parameter determination, TPU, PDMS, damper structures

1. Introduction

Damping systems are indispensable in daily life and are applied in various products as in cars to make driving comfortable, machines to reduce noise, and sport equipment (e.g., shoes for protection of human joints) [1]. The (motion) damping mechanism can be separated into active, passive, as well as in a combination of both [2]. Active damping is required, because passive damping causes an increase of the system's transmissibility at high frequencies [3]. Furthermore, active damping enables nearly perfect damping of the system over the entire application range, for instance in sport cars [4]. In general, multi-material compositions with properties adjustable by a physical field (e.g., magnetic, electric, thermal, etc.) are used in active damping. The most common materials are magnetically polarizable particle-filled elastomers, which can change their behavior rapidly, continuously, and reversibly by an applied magnetic field [2, 5]. The capability of an elastomer to adjust its behavior within magnetic fields is measured by the ratio of the magneto-induced shear modulus and the zero-field modulus ($\Delta G/G0$) and is the characterizing parameter for the relative magnetorheological (MR) effect [2]. The MR effect exhibit the

(same) inherent viscoelastic behavior as the matrix material (elastomer) and, therefore, is a function of loading rate (time) and temperature. In addition, the effect is more pronounced when the elastomer is softer (even higher for magnetorheological fluids). It can be shown, that the softer (compliant mechanical behavior) the matrix, the higher the MR effect, due to the higher unrestricted movement of the particles within the matrix elastomer [6, 2]. However, material data of the physical field dependent material properties are not easily available, consequently it is a vivid field of research to gain deep insights of the interplay of the inherent viscoelasticity, the particles, and the physical field. In contrast, passive damping is a response of the material due to a disturbance in the system [2]. The damping properties depend on the material composition and depends highly on temperature and frequency; however, they are usually not adjustable during application. Furthermore, the complex dynamic modulus of elastomers can be split in a real and an imaginary part (storage Young's modulus E′ and loss Young's modulus E′′). E′′ as well as the loss factor ($\tan\delta = E'/E''$) are directly related to the damping capacity (ratio of dissipation energy and elastic energy, U_d/U_e), the higher E′′ ($\tan\delta$), the higher the damping [7, 8, 9]. For elastomer-appropriate design of damping systems, polymer product engineering methodologies are needed. Otherwise, the utilization of both active and passive dampers in engineering applications is limited to non-structural parts.

To overcome this limitation, this work applies systematic experimental and material parameter determination procedures based on methods published in [10], [11] and [12] including a case study. The objective was the analysis of the damping behavior of silicone elastomer rubbers (PDMS) and thermoplastic poly(urethanes) (TPU). A methodology is presented including the hyper- as well as viscoelastic characterization, and material parameter determination for finite element analyses (FEA). This procedure is applied to substitute a conventional spring-dashpot damping system (coil-over shock absorber) of a model car. The shock absorbers of a remote-controlled car were redesigned by replacing the spring-dashpot system (structural damping) with an elastomer (material damping). Finite element (FE) calculations of a ball-drop test were performed with material data obtained from hyper- as well as viscoelastic characterizations. For validation purposes of the FE model, rebound resilience experiments were conducted and compared with the simulated results. Finally, the state-of-the-art as well as the new shock absorbers characteristics were examined.

2. Materials and Methods

Figure 1 shows the workflow of the applied methodology. It covers all aspects of polymer product engineering from material and validation tests for FEA to product tests. First, the hyperelastic and viscoelastic behaviors of the TPU and PDMS were examined and by applying appropriate data reduction methods, the parameters for constitutive models were determined. These parameters were implemented in structural analyses performed with finite element methods (FEM). The specimens and damping elements made of PDMS were molded under laboratory conditions and these made of TPU were provided from the material supplier. Damping elements for the conducted application case study of a model car were also prepared with these materials.

2.1 Materials

Two types of elastomeric materials were investigated, (i) thermoplastic poly(urethane) (TPU), and (ii) silicone rubber blends (PDMS). With these materials a wide range of thermo-mechanical properties with different damping properties are covered (e.g., hardness ranges from Shore D50 down to Shore 00-30). Furthermore, the examined materials are ideal damping materials and are materials of choice for damping elements. For instance, TPUs are utilized for shoe soles to enhance comfort [1], and silicone rubbers in optical systems or for sensors [13].

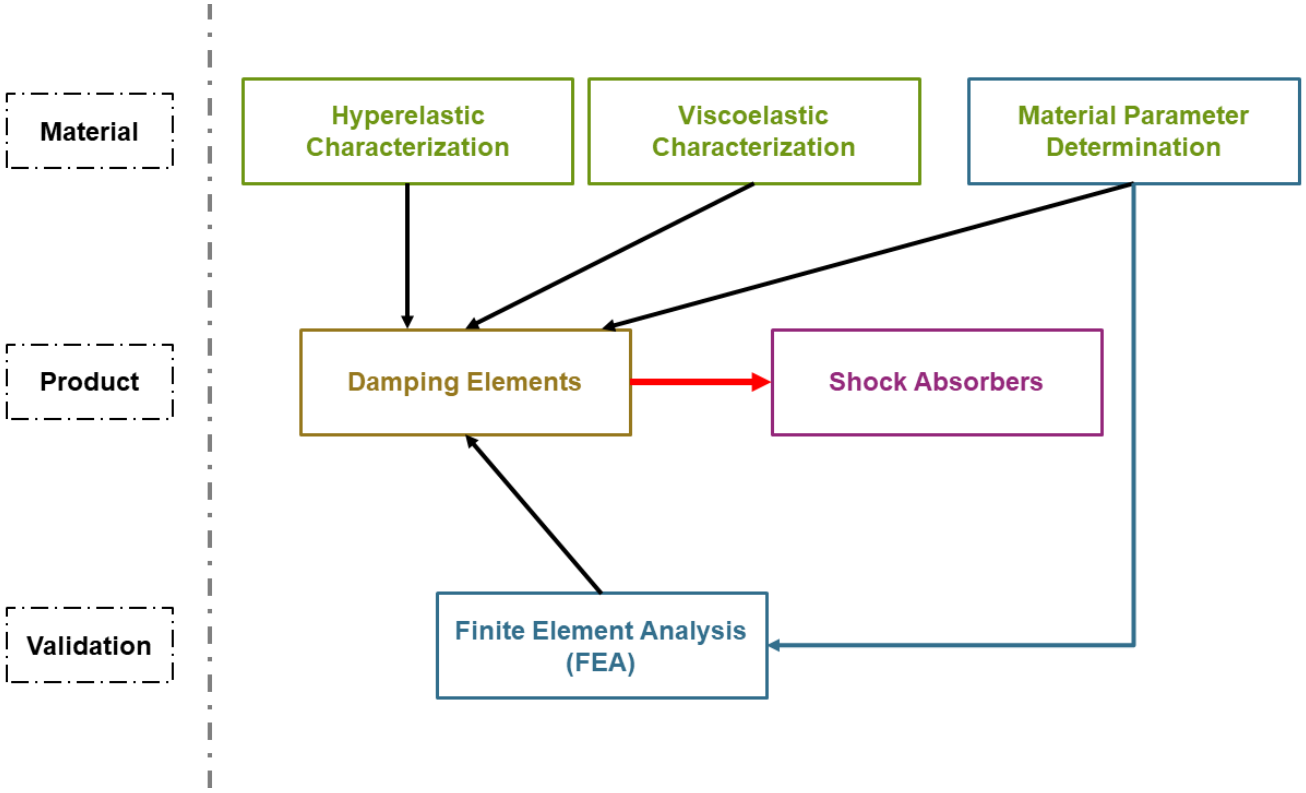

Figure 1: Schematic illustration of the applied workflow.

Both TPUs, are based on aromatic isocyanate and poly(carbonatpolyol) and were provided by the material supplier (DMH Dichtungs- und Maschinenhandel GmbH, Styria, AUT) with a hardness of Shore D46 (TPU1-MDx) and D50 (TPU1). The TPU1-MDx was filled with iron (Fe) particles. The purpose of the fillers is to enable detectability, electro-active, and magneto-active behaviors, even applications in contactless communication and data transfer are feasible. Furthermore, TPU1 filled with Fe particles is particularly interesting for active damping applications. In general, both TPUs are developed for a service temperature range from -20°C up to 115°C, are FDA certified, and are resistant against hot water, oils, ozone, as well as synthetic and natural ester.

For the silicone rubber blends a mixture of two different poly(dimethylsiloxane) (PDMS) with Shore 00-30 (Ecoflex®, from Smooth-on Inc., Pennsylvania, USA; referred to as Ecoflex in the following) and Shore A43 (Sylgard™ 184 from DowDuPont Inc., Wilmington, USA; referred to as Sylgard in the following) were casted as sheets and cylinders. Both materials have similar damping capacities (or loss factors tanδ) but different stiffnesses (Young's moduli). However, they are miscible resulting in blends with varying stiffnesses depending on the mixing ratio [14]. For this work one blend in addition to the neat PDMS was characterized and analyzed. The PDMS formulations were named after the incorporated fraction of Ecoflex starting from neat Ecoflex (**100E**), blend of 50w% (**50E**), and neat Sylgard (**0E**).

2.2 Design Concept

The state-of-the-art damping elements (coil-over shock absorber) of a remote-controlled car (Traxxas BANDIT [15]) were redesigned by replacing the spring-dashpot system (structural damping) with an elastomer damper (material damping). The differentiation of structural and material damping is made based on the mechanics of energy dissipation (damping). In **Figure 2**, the different damping mechanisms and their components are illustrated. The complex modulus E* (or also G*) of the elastomer is loading rate and temperature dependent and, ultimately, tuned for the application loading range. In **Figure**

3(a) the coil-over shock absorbers of the remote-controlled car are shown and in **Figure 3(b)** the damping element utilizing material damping including their components.

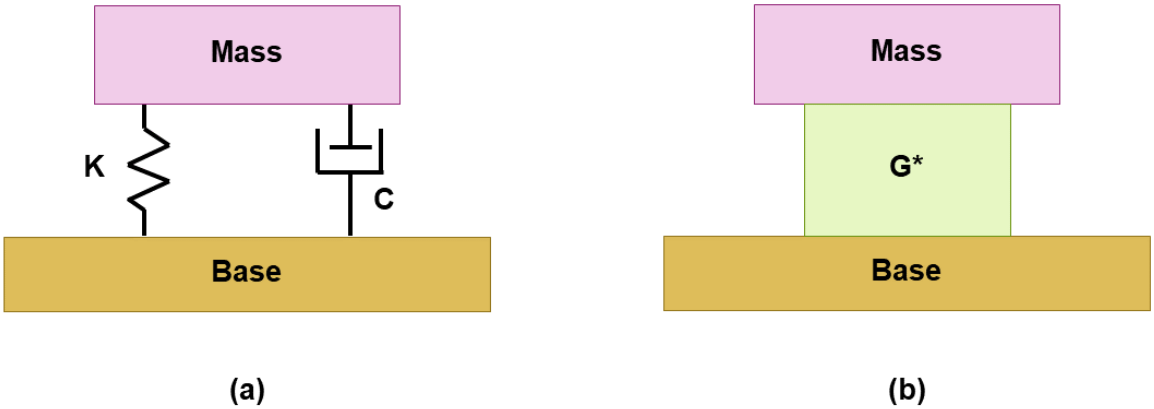

Figure 2: (a) Structural damping with a spring (K) and a dash-pot (C); **(b)** equivalent damping of structural system, but made of elastomers with inherent viscoelasticity (complex shear modulus G* is loading rate as well as temperature dependent).

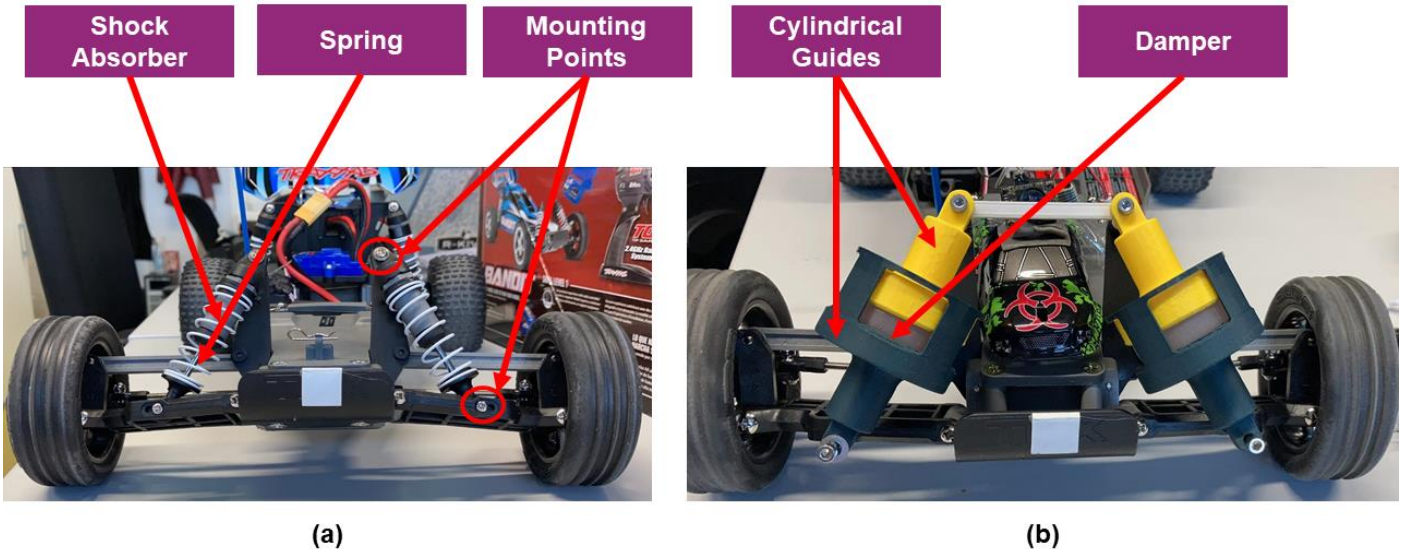

Figure 3: Front view of the remote-controlled car with **(a)** the original shock absorbers and **(b)** the new designed ones.

The coil-over shock absorber is made of ten parts, while the proposed damping element is made of three. For the damping element, the original screw fixations were used as shown in **Figure 3 (a)** and **(b)**. The elastomer damper was designed as a cylinder with a diameter of ⌀35mm and a height of 20mm. To hold the damper in place, the damper was constrained by two 3D-printed cylinders made of poly(lactidacid) (PLA) (yellow and dark green cylindrical guides shown in **Figure 3 (b)**). To ensure a consistent load path, the structure of the damping element is self-supporting. The silicone elastomer blends (100E, 50E, and 0E) are depicted in **Figure 4**. TPU dampers were investigated as hollow cylinders to ensure that the apparent stiffness (i.e., structural stiffness, cf. [16]) range is comparable to that of PDMS. Therefore, the cylinders were drilled with holes of ⌀13mm and ⌀6mm diameter. **Figure 5 (a)** illustrates the axis where the holes were drilled with 90° offset of

holes with equal diameters, consequently the angle between the ⌀13mm hole and the ⌀6mm holes is 45°. **Figure 5 (b)** shows the prepared TPU dampers.

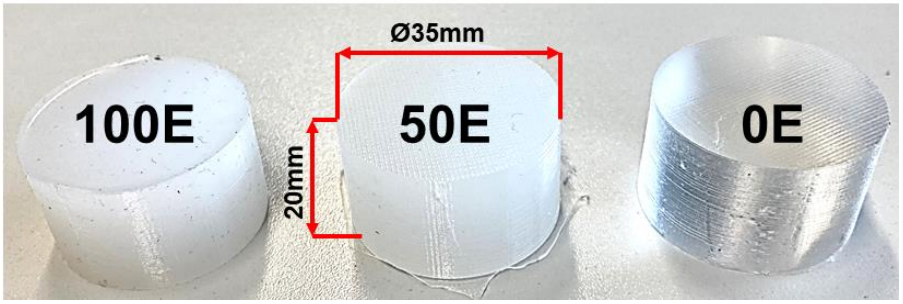

Figure 4: PDMS-dampers: 100E (left), 50E (middle), 0E (right).

Figure 5: (a) Diameter and location of the drilled holes with the respective diameters; **(b)** blue: TPU1-MDx damper; red: TPU1 damper.

2.3 Methods

For the hyper- and viscoelastic characterization, the TPU specimens were stamped from molded plates and the PDMS blends were casted under laboratory conditions. The uniaxial tension tests were performed with an electromechanical testing system (TestBench, Bose Corp., ElectroForce Systems Group, MN, US) under isothermal conditions at room temperature and three loading rates (0.1 mm/s; 1 mm/s; 10 mm/s). The specimen geometry as well as the setup are shown in **Figure 6**. The measurement was displacement controlled and the force was recorded with a 440N load cell (WMC-100lbf, Interface Inc., AZ, US). The strains were derived by a LVDT (linear variable differential transformer, AD598, Analog Devices Inc., MA, US). Prior to testing, the specimens were clamped with a clamping length of 20mm and to compensate the occurring clamping force, the specimens were elongated until the force was equal to zero. Afterwards, the initial length l_0 of the specimen was measured for further analyses and measurement was started displacement controlled at constant loading rate under isothermal conditions.

The material parameter determination was performed by assuming incompressibility and measuring the uniaxial characteristics. As shown in **Figure 7 (b)** all experimental data were fitted iteratively to identify the parameters C_1 and C_2 of the Mooney-Rivlin model (see Equation (1)) for $\lambda_1 = \lambda$ (stretch in loading direction), and $\lambda_2 = \lambda_3 = 1/(\lambda)^{1/2}$ is shown in **Figure 7 (a)**.

$$\sigma = \frac{1}{2\left(\lambda - \frac{1}{\lambda^2}\right)} = C_1 + \frac{1}{\lambda} C_2 \qquad (1)$$

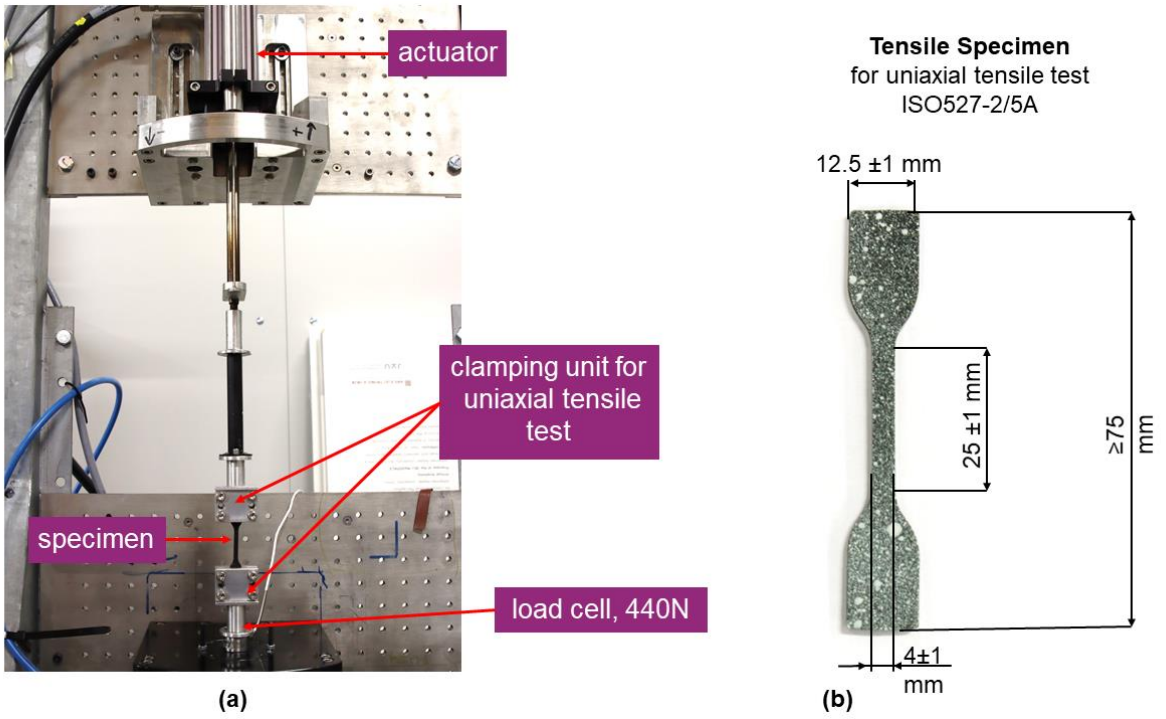

Figure 6: (a) Set-up of the uniaxial tensile test; **(b)** Geometry of the used specimen according to DIN-EN-ISO-527-5A.

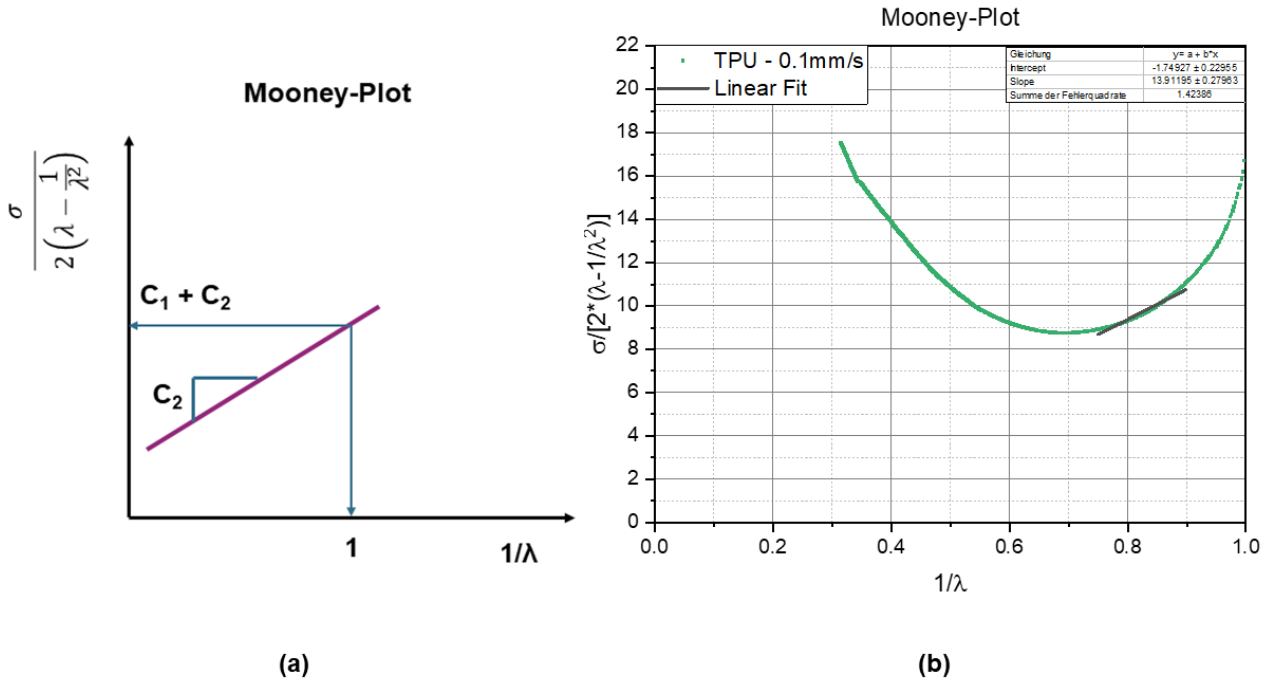

Figure 7: (a) Schematic representation of the Mooney-Plot; **(b)** Mooney-Plot and estimated material parameters for the constitutive law.

This model does not capture the temperature dependency of hyperelastic materials. Therefore, a dynamic thermomechanical analyses (DTMA) was performed to determine the temperature and frequency dependent storage and loss moduli (E′ and E′′), respectively the loss factor tanδ = E′′/E′. The dynamic thermomechanical behavior of the TPUs were analyzed under uniaxial loading, at a temperature range from -80°C to +80°C and at frequencies from 0.5Hz to 50Hz. For the PDMS-blends the temperature range was from -30°C to 40°C at a frequency range from 5Hz to 18Hz. DTMA was performed with an

Eplexor 500N (Netzsch-Gerätebau GmbH, Selb, DEU) and started at the lowest temperature and was increased in steps of 5K for the TPUs and 10K for the PDMS-blends.

The dynamic wave amplitude was a sine wave with a mean strain level of 20% (TPUs) and 0.5% (PDMS-blends) and a dynamic peak-to-peak (p-p) amplitude of 2%. In order to compensate the thermal elongation a holding force of 0.5 N was set and the initial length at isothermal conditions was measured. At each temperature pre-cycles were performed to avoid stress softening effects. **Figure 8 (a)** shows the temperature dependent storage E′ and loss moduli E′′ at three excitation frequencies (0.5Hz, 5Hz, 50Hz) and **Figure 8 (b)** illustrates the frequency dependent E′ master-curve for the reference temperature T_{ref} of 25°C. Also, the data from the measured experimental window are shown in **Figure 8 (b)** revealing decreasing E′ with increasing temperature. According to the time-temperature superposition principle the experimental data at lower temperatures are equivalent to high frequency data (shift to right) and vice versa (cf. [17]).

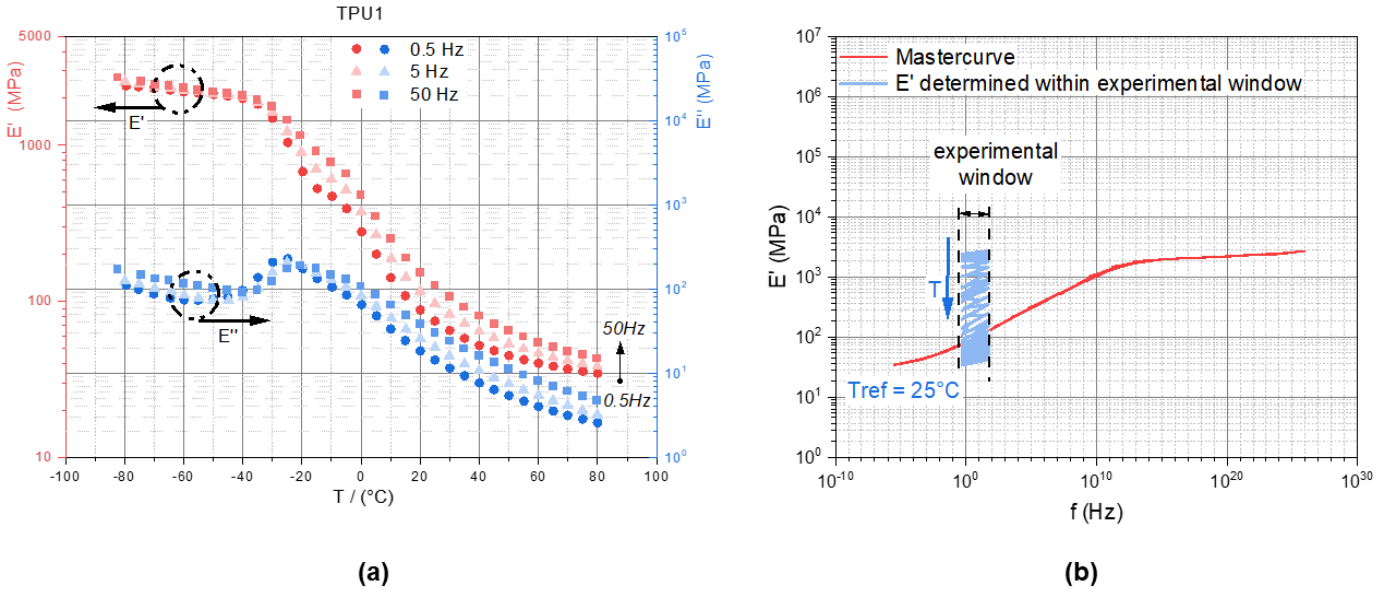

Figure 8: DTMA analyses for TPU1; **(a)** loading frequency and temperature dependent storage and loss moduli (E′ and E′′); **(b)** calculated master curve with a reference temperature of 25°C.

For the characterization of the damping capacity, the rebound resilience was measured. The rebound resilience (ratio of rebound height and initial drop height, h/h_0) is related to the damping capacity (ratio of dissipated energy and elastic energy, U_d/U_e) and, in general, the higher the rebound resilience, the lower the damping of the material within the range of 0 (ideal damper) and 1 (ideal elastic). The measurement of the rebound resilience was performed with a custom-made test set-up based on a pendulum impact tester (ZwickRoell, Ulm, DEU) with a 0.5 J pendulum. Position of the pendulum was recorded by a rotary encoder (Kübler, Villingen-Schweninngen, DEU) connected to a GEN2i (Genisis High Speed Mainframe with integrated PC, HBM, Vienna, AUT) for data acquisition. The procedure of the measurement was that the pendulum was placed at a 0° position and the specimen was placed centered to the pendulum at impact. Depending on the specimen size the clamping base variated in height and depth. The specimen is supported on the edgewise frontal surface and on the backside (see **Figure 9**). It was important that the specimen is placed and positioned so that the contact of the specimen with the pendulum is at the 0° position for higher accuracy of the impact speed. Finally, the measurement was performed by dropping the pendulum on the specimen and was repeated five times for each temperature.

The TPU specimens were rectangular plates (50 mm x 40 mm) with a thickness of 6.30mm, which were injection moulded by DMH Dichtungs- und Maschinenhandel

(Styria, AUT). The PDMS blends were casted cylinders with a diameter of ⌀60mm and a height of 30mm. The measurements were performed at -20°C, 22°C and 60°C for the TPUs and at -50°C, -30°C, -25°C, 0°C, 30°C and 50°C for the PDMS blends. Different temperature ranges were selected for the examined materials as TPU has a glass transition temperature Tg of -20°C (see **Figure 8 (a)**) limiting the low temperature applicability. The specimens were conditioned for min. 1h at each temperature in the temperature chamber (CTS Clima Temperatur Systeme GmbH, Jennersdorf, AUT). Once the measurement was conducted, the angular position was recorded and height, impact speed as well as impact force derived. The conversion from the recorded angular position to the height of the pendulum is given in Equation (2). Subsequently, the rebound resilience was determined by the ratio of rebound height h and initial height h_0 of the pendulum (see Equation (3)).

$$h = L - L * cos\left(B * \frac{\pi}{180}\right) \tag{2}$$

h…actual height [m]
h_0…height of the start position [m]
L…length of the pendulum [m]
B…measured angular data [rad]

$$rebound\ resilience = \frac{h}{h_0} \tag{3}$$

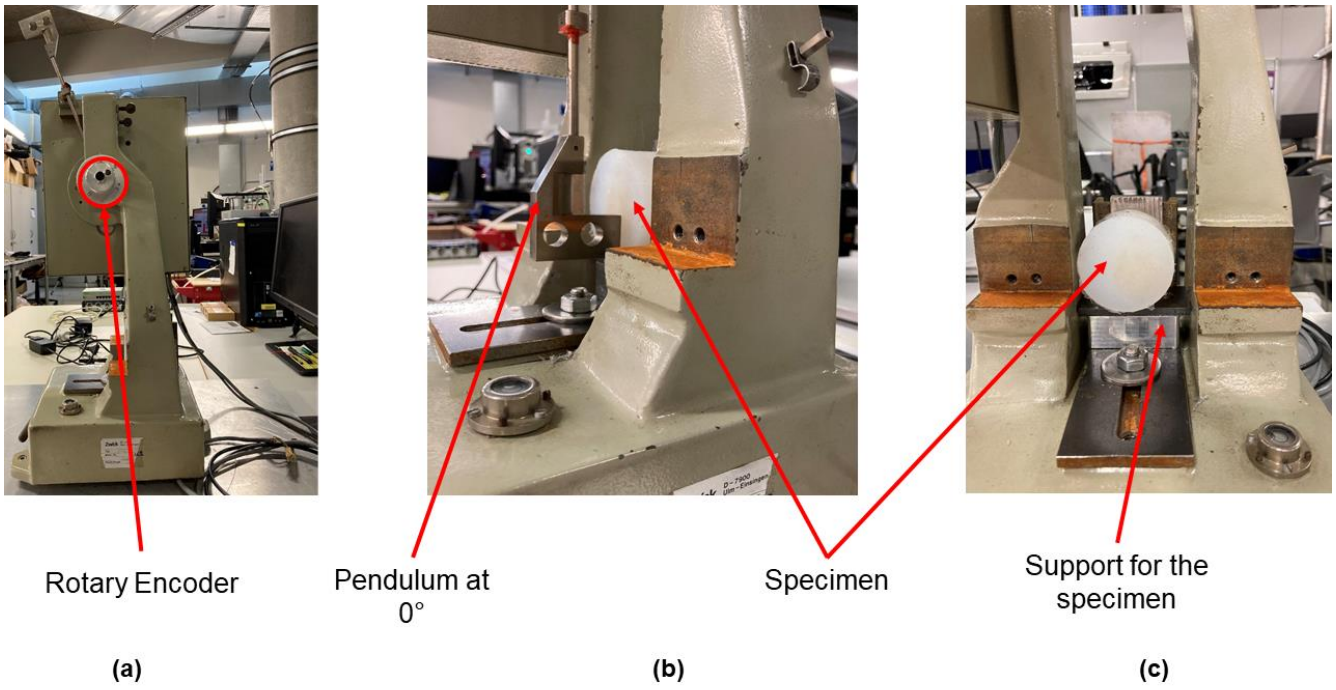

Figure 9: (a) Pendulum at start position; **(b)** pendulum and a PDMS blend at 0° position; **(c)** specimen and the clamping.

2.4 FE-Calculations

The finite element (FE) simulation of a ball drop test configuration was performed with a ball of diameter 29mm dropping onto a hyperelastic cylinder. The FE model was validated by the rebound resilience experiments. The model was set-up in Abaqus 2020 (Dassault Systèmes Simulia) and is shown in **Figure 10 (a)**. The initial position of the ball was 430mm above the damper. With this height and the mass of the ball the impact energy

is equal to the experimental setup of the rebound resilience. The step was primarily set as dynamic, explicit with a time of 1.5s. For the ball, the interaction was of the type general contact (explicit). All part interactions were set to "all with itself" with frictionless tangential behavior. The boundary conditions at the bottom part of the damper were fixed in all directions of freedom and gravitational force ($g = 9.81 m/s^2$) was applied in z-direction.

Damping was modelled with Rayleigh damping (α, β parameters) [18] and hyperelastic material behavior with Mooney-Rivlin constitutive law. Due to large deformation of the rubber, the nonlinear geometric function is enabled. The ball was modelled linear elastic with parameters of steel ($E = 210GPa$, $\nu=0.33$, $\varrho=7830kg/m^3$). For the ball as well as the damper an 8-node linear brick with reduced integration and hourglass control(C3D8R) was used (as shown in **Figure 10 (b)**). The approximate global size was set to 3mm for the damper and to 0.71mm for the ball. Curvature control was used for applying the global seeds. The maximum deviation factor was set to 0.1 as is set by default in Abaqus CAE. **Figure 10 (c)** shows the first impact of the ball on the damper. For validation of the results, the displacement of the ball in z-direction was used to calculate the rebound resilience according to Equation (3).

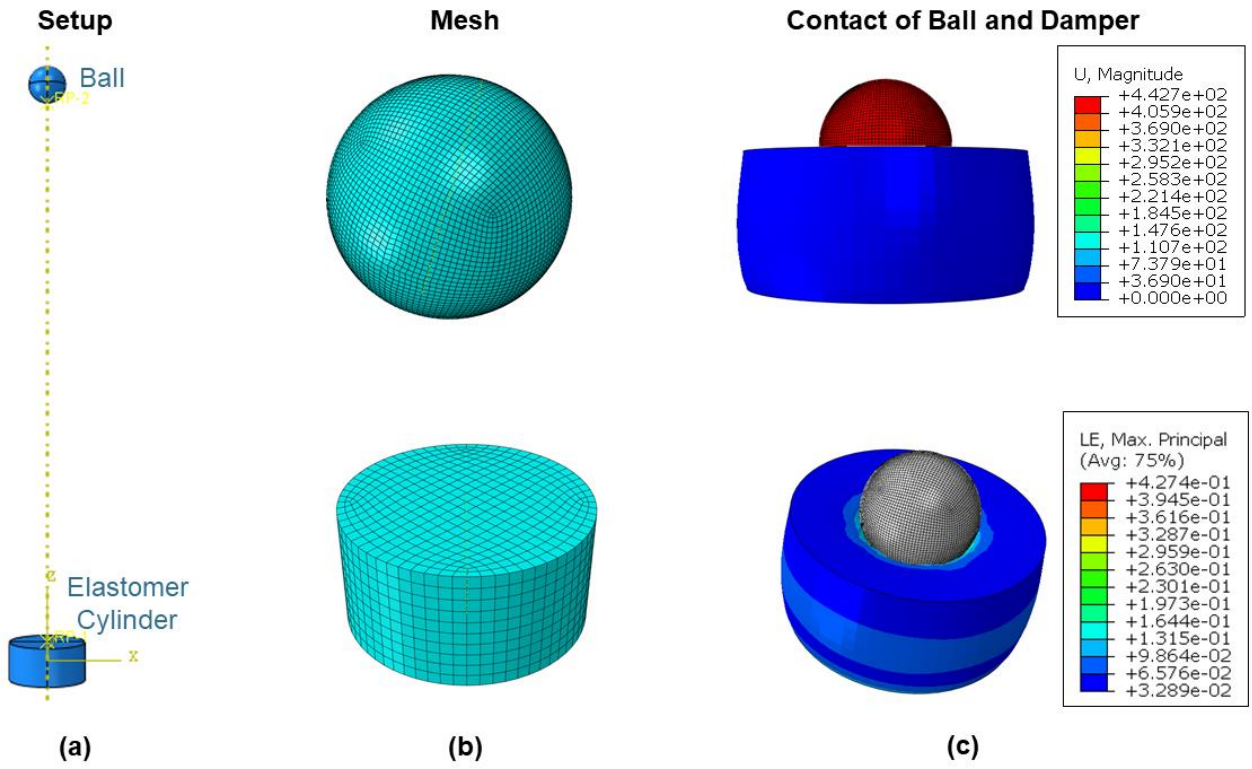

Figure 10: (a) Setup of the ball-drop test; **(b)** illustration of the meshed parts; **(c)** different viewports of the damper loaded with the ball.

2.5 Component testing

The coil-over shock absorber and the damping element were tested under cyclic loading to determine the mechanical performance characteristics. This measurement was performed with the hydraulic testing system MTS 852 damper test system (MTS Systems Corporation, Eden Prairie, MN, USA) including a 10kN load cell (Force Transducer-2200lbf Version1, MTS System Corporation 14000 Technology Drive ® Eden Prairie, MN,

US). The setup with its main components including the load cell, clamping unit, as well as actuator is shown in **Figure 11**.

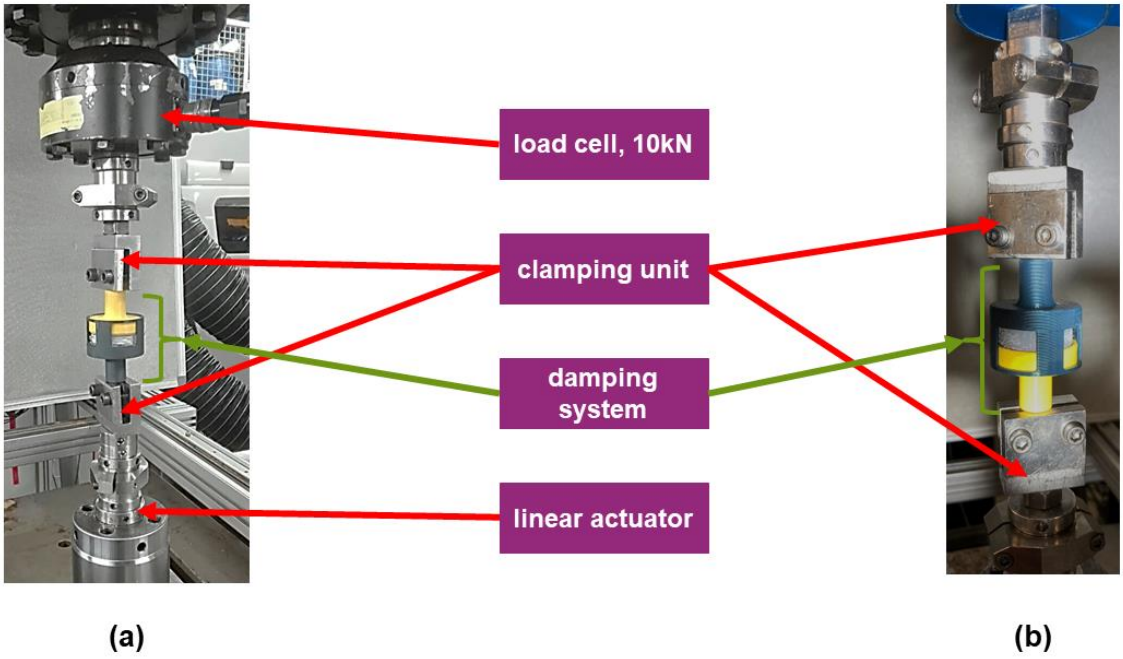

Figure 11: Setup of the component test. **(a)** shows the new designed damping system with a 0E damper as well as the used load cell, the clamping, and the linear actuator of the used testing machine; **(b)** shows the clamped damping system with a 0E damper and the clamping.

The testing procedure was performed under displacement-controlled cyclic sine wave loading with a dynamic p-p amplitude of 0.4% and mean strain level of 10%. **Figure 12** shows the loading definition of the testing procedure. First, the materials were compressed to the mean strain level and held until stress relaxation was over meaning that mean stress reached a constant level. Then, the dynamic wave amplitude started with 20 sine cycles. Finally, the materials were further compressed to -15% strain (TPUs) and -30% strain (PDMS-blends). These strain levels were conducted in order to investigate the compression behavior of the dampers.

In the following the results of the experimental and numerical analyses are presented starting with the hyper- as well as viscoelastic (DTMA) characterizations, followed by the material parameter determination for the Mooney-Rivlin constitutive model, and the results of the rebound resilience. The results of the rebound resilience are compared to simulated data. At the end, the component testing results of the structural performance characterization under cycling loading are presented and discussed.

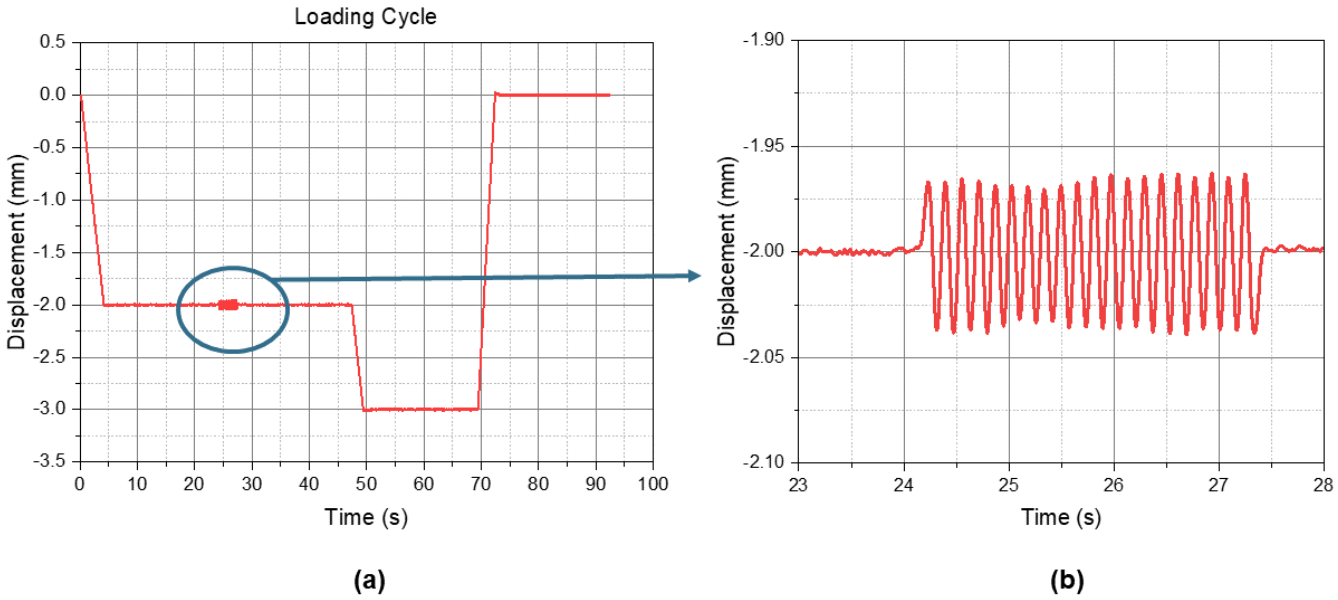

Figure 12: Displacement controlled cycles for the tested components. **(a)** shows the complete load cycle and **(b)** illustrates the sine load.

3. Results

The stress-strain curves were necessary for the calculation of the Mooney-Rivlin parameter C_1 and C_2. For the calculation of the parameters, C_1 and C_2 the data were reduced to 25% strain, due to the fact that the accuracy of the Mooney-Rivlin constitutive law is higher at small strains. Diagrams of **Figure 13 (a)**, **(c)** and **(e)** show the stress-strain curves of the examined TPUs, which behave very similar. These results show that the iron particles in the TPU1-MDx have no influence on the tensile behavior.

In **Figure 13 (b)**, **(d)**, and **(f)**, the stress-strain curves of the PDMS formulations are shown. For all loading rates the 0E (100% Sylgard) was the stiffest material within the PDMS formulations. In general, the TPUs (see **Figure 13**) were stiffer than the PDMS (stress, σ of 0E at strain, ε = 25% (0.1mm/s) = 0.30MPa, σ of TPU1 at ε = 25% (0.1mm/s) = 9MPa). The stress-strain characteristic of the 50E blend is closer to that of the 100E but stiffer.

The determined and validated Mooney-Rivlin material parameters are listed in **Table 1** for the TPUs and in **Table 2** for the PDMS formulations.

Table 3: Determined material parameters of the TPUs.

Mooney-Rivlin Parameter	TPU1	TPU1-MDx
C1	0.000178	1.61
C2	9.74	7.86

Table 4: Determined material parameters of the PDMS-formulations.

Mooney-Rivlin Parameter	0E (100% Sylgard)	50E (50w% Ecoflex)	100E (100% Ecoflex)
C1	0.35	0.081	0.0068
C2	-0.13	-0.015	0.0017

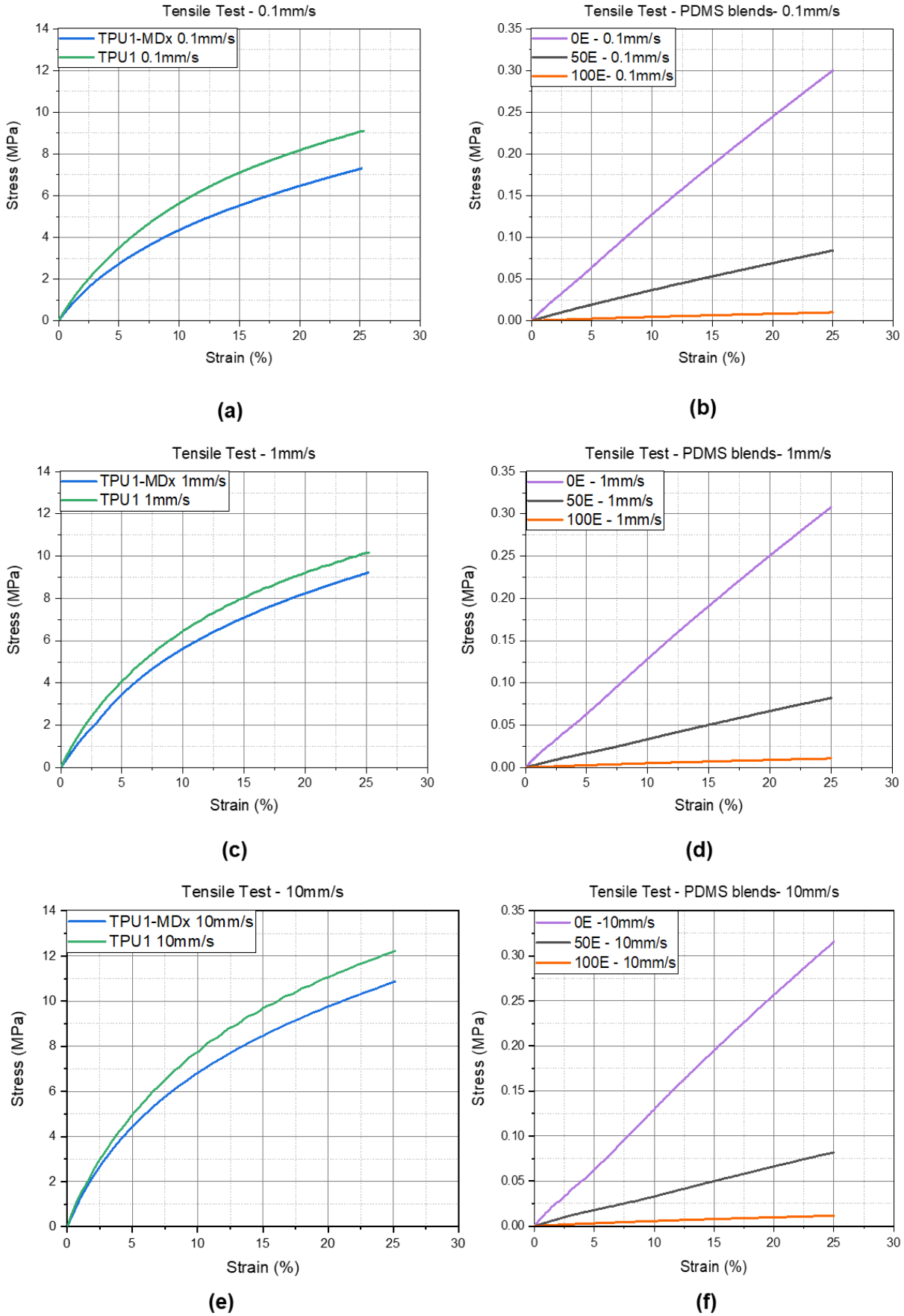

Figure 13: Stress-strain data from the evaluated tensile test of the TPUs and PDMS mixtures. **(a)** and **(b)** 0.1mm/s loading rate; **(c)** and **(d)** 1mm/s loading rate; **(e)** and **(f)** 10mm/s loading rate.

The characterization of the loading rate and temperature dependency of the TPUs under dynamic thermomechanical loading confirmed that the Fe particles did not influence the material behavior significantly. In **Figure 14 (a)** and **(b)**, the loss Young's modulus E'' data of TPU1 and TPU1-MDx are shown. Similar characteristics were measured. Only the temperatures at the maxima of E'' were shifted indicating that the glass transition temperatures were affected by the Fe particles. The TPU1 revealed the highest E'' at -25°C (**Figure 14 (a)**) while the maximum E'' of TPU1-MDx was at -22°C (**Figure 14 (b)**). So, the glass transition of TPU1-MDx occurred at higher temperature and, thus, limiting the low temperature resilience of the material.

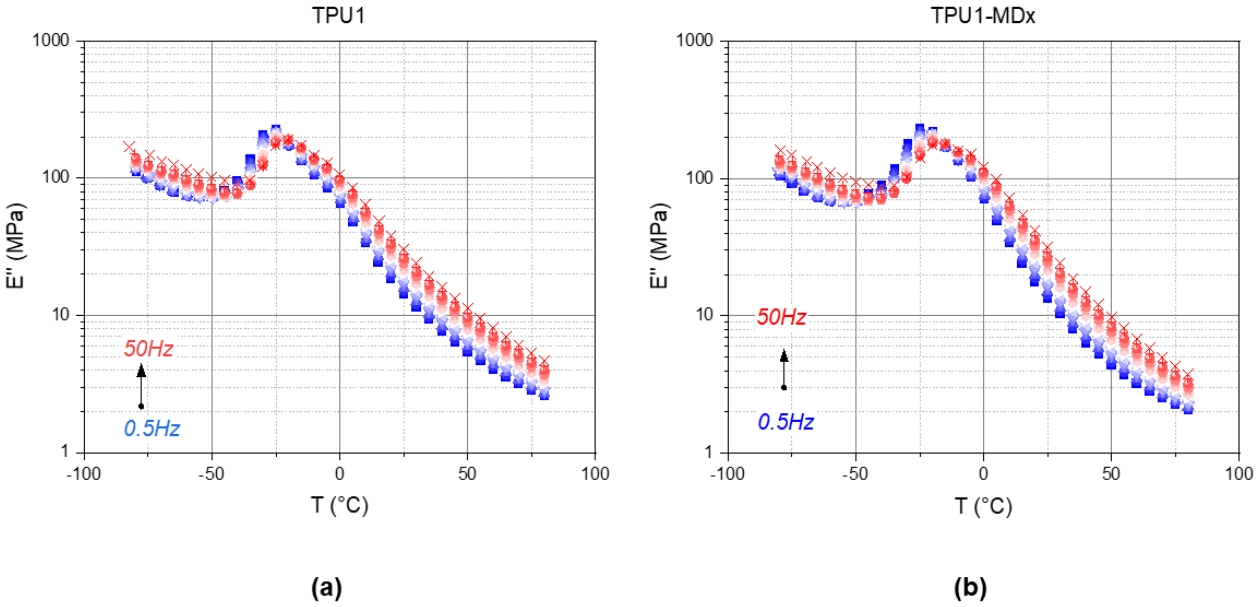

Figure 14: Loss modulus (E'') over temperature. **(a)** TPU1; **(b)** TPU1-MDx.

Figure 15 (a) and **(b)** illustrate the loss modulus (E'') over temperature for the 0E **(a)** and the 100E **(b)** blends, respectively. The loss modulus E'' of the 0E blend decreased with increasing temperature, while the 100E blend revealed nearly constant E'' across the experimental temperature range. However, maxima of E'' were obtained for all excitation frequencies at 20°C. At temperatures above 40°C, the E'' of 100E for all frequencies were approaching towards a value of 0.01MPa. This is an important insight for the damper material selection in high frequency vibration applications.

The results of the experimentally determined rebound resilience are shown in **Figure 17**. In this diagram, the rebound resilience of the first rebound for each temperature is shown and, in the following, compared to predicted data. The 50E PDMS-blend has the highest rebound resilience of all material formulation over the tested temperature range. This means that the damping capacity of 50E are reduced compared to the neat silicone elastomers Sylgard and Ecoflex. It is also interesting that the 100E has the lowest value at 0°C while the results of the DTMA revealed that the highest E'' is at 20°C (see **Figure 15 (b)**). As mentioned earlier, the difference of 100E's loss modulus E'' data over the whole temperature range was low and, therefore, the direct comparison can lead to non-conclusive results. This has to be analyzed in detail. In contrary, the 0E exhibited the lowest rebound resilience at -30°C and was consistent with the results of the DTMA (see **Figure 15 (a)**). Generally, the rebound resilience of 0E and 100E neat PDMS were much lower (i.e., higher damping capacity U_d/U_e) compared to the 50E. Furthermore, similar rebound resilience data were measured for the neat PDMS. This trend confirmed that the loss factor tanδ (E''/E') of both materials are similar within the range of 0.05 and 0.3 depending on

the testing temperature (see **Figure 16**). The Young's moduli of 100E (@20°C) and of 0E were in the range of 0.1MPa and 1MPa, respectively.

The TPUs exhibited similar rebound resilience behavior between 22°C and 60°C, however their characteristics below -20°C diverge significantly. This was in accordance with the shift of the glass transition temperature with the incorporation of Fe particles in TPU1 (cf. **Figure 14 (a)** and **(b)**) and indicated the limitation of the low temperature resilience of TPU1-MDx.

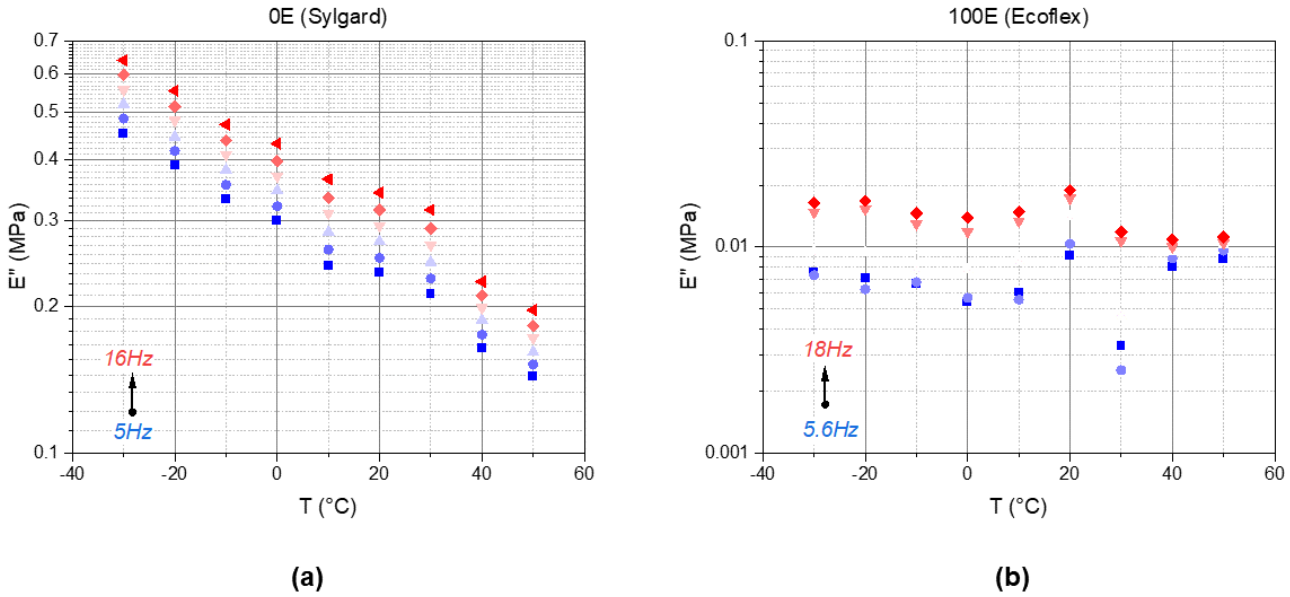

Figure 15: Loss modulus (E'') over temperature: **(a)** 0E (100% Sylgard); **(b)** 100E (100% Ecoflex).

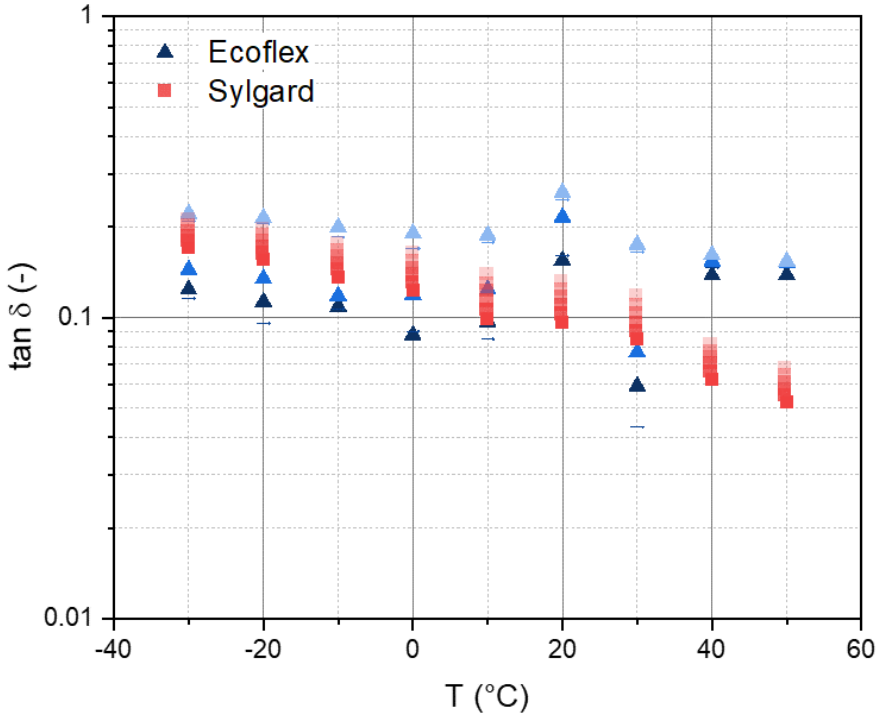

Figure 16: tanδ over temperature of the 100E (Ecoflex) and the 0E (Sylgard) PDMS.

Overall, the TPUs revealed the best damping capacity (lowest rebound resilience) of the characterized materials. For low temperature applications up to -20°C, TPU1 is a potential candidate material for dampers.

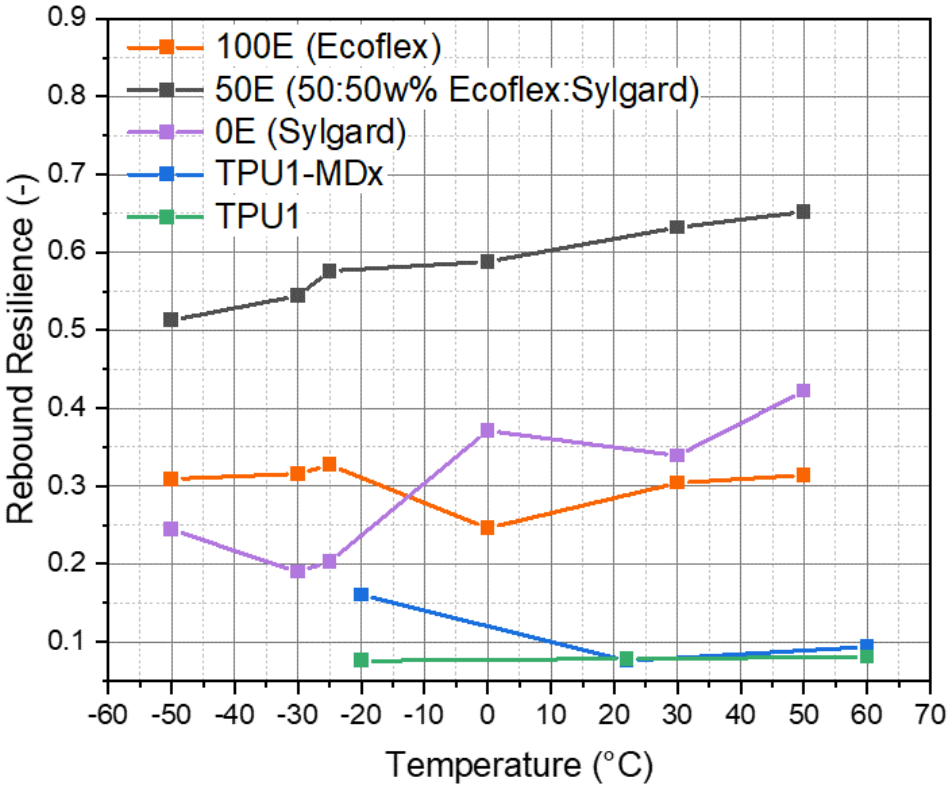

Figure 17: Rebound resilience (h/h_0) of all characterized materials.

With the material parameters determined experimentally, the FE simulation of the ball-drop test configuration for the PDMS-blends were conducted. In **Figure 18 (a)** and **(b)**, the results of 0E and 100E, respectively, are presented for comparative analyses. The black curve represents the measured rebound height and the red curve the results of the simulation. Generally, good agreements were found between the FE and the experimentally determined data. For 0E PDMS, the maximum rebound resilience of the experiment was 0.728 and the predicted was 0.730. Only the impact time was shifted by a small fraction of a second to the right about 0.023s. For 100E, the experimental maximum rebound resilience was at 0.495 and the FE result was at 0.535. However, the difference of the impact times from simulation and experiment was smaller compared to the simulation of the 0E (0.005s).

The results of the component tests are presented as loading displacement and response load versus time curves (see **Figure 19**). The diagram shows that there is no difference between the first and the second measurement, neither for the PDMS-formulations nor for the coil-over shock absorber. As expected, the 0E PDMS formulation was the stiffest material and high response loads are obtained. The 100E PDMS was the softest material, accordingly. The characteristics of 50E PDMS-blend was closer to 0E rather than 100E confirming the results of the uniaxial testing (cf. **Figure 13**).

Comparing the measurements of the TPUs, differences in the damper response load between the 1st and the 2nd measurement were observed for both TPUs. This difference was related to the compression set of the TPUs between the measurements.

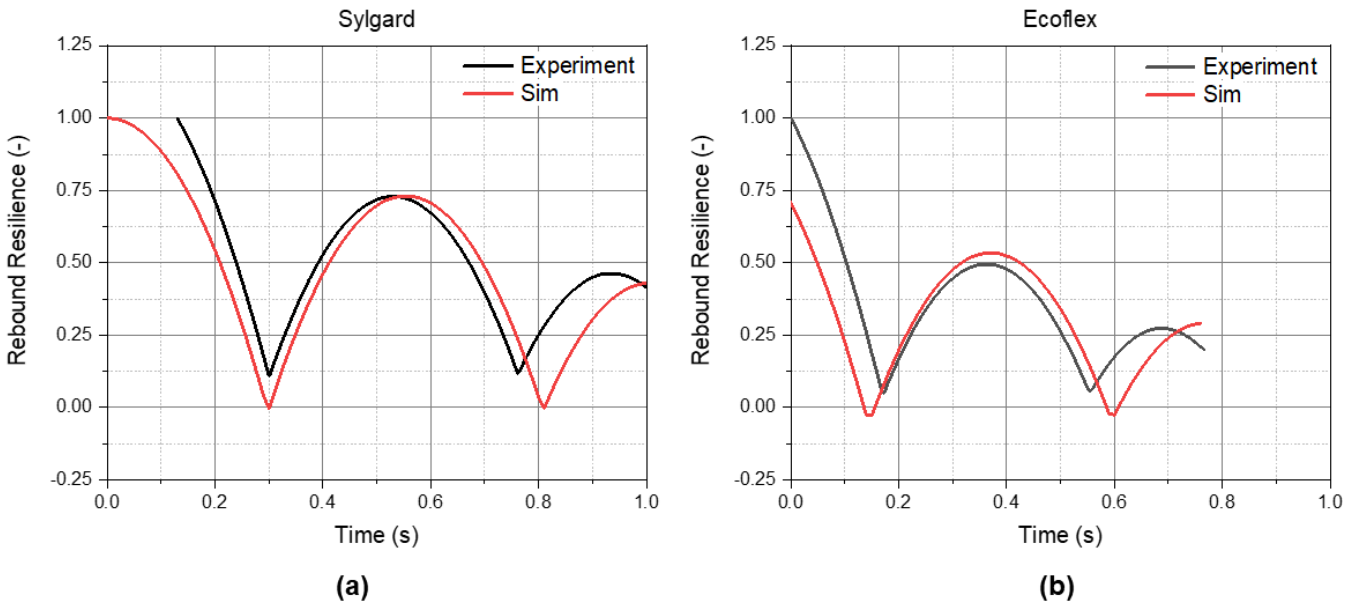

Figure 18: Comparison of the measured rebound resilience and the FE-calculated, **(a)** for the 0E PDMS Sylgard and **(b)** for the 100E PDMS Ecoflex.

In general, the system with the TPU1 damper shows a softer behavior compared the TPU1-MDx system. For the TPU1-MDx the difference between the 2nd and 3rd measurement shows a stress-softening effect, which is probably related to the interface weakening between the Fe particles and the TPU-matrix. As a result, the damping capacity was affected and with increasing number of applied loading, the damping was reduced. This effect has to be analyzed in future.

4. Discussion

The results of the hyper- and viscoelastic characterizations for the TPUs showed that the Fe particles have low influence on the mechanical behavior of the TPU1-MDx. Also, the results of the experimentally determined rebound resilience were within the same range, except below 20°C. At this temperature the TPU1 damps better than the TPU1-MDx. This was related to the shifted glass transition temperature of TPU1-MDx to higher temperatures with the incorporation of Fe particles. The cyclic component tests showed that the TPU1-MDx exhibited higher compressive loads compared to the TPU1. Consequently, the Fe particles were reinforcing the material in compression while the tension behavior remains unchanged. By comparing the 2nd and the 3rd measurements, only the TPU1-MDx showed a stress-softening effect, which is not analyzed in detail and has to be conducted in future. This effect is related to the interface weakening between the Fe particles and the TPU-matrix.

The uniaxial tensile tests of the PDMS-blends revealed that the desired (tailored) blend properties can be achieved. The 0E (Sylgard) was the stiffest blend and the 100E (Ecoflex) was the softest. Interestingly, the 50E (mixing ratio of 50:50) exhibited a tensile behavior similar to 100E rather than the 0E neat PDMS, however, with the

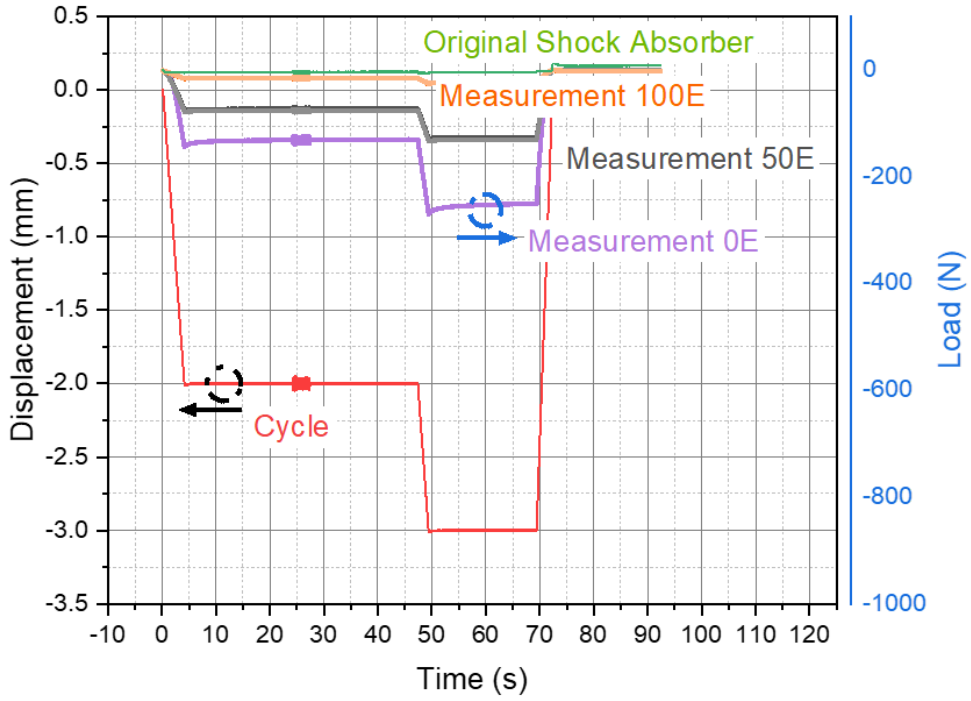

Figure 19: Load cycle of the PDMS-blends and the original shock absorbers as well as the load curves of the analyzed PDMS-blend dampers.

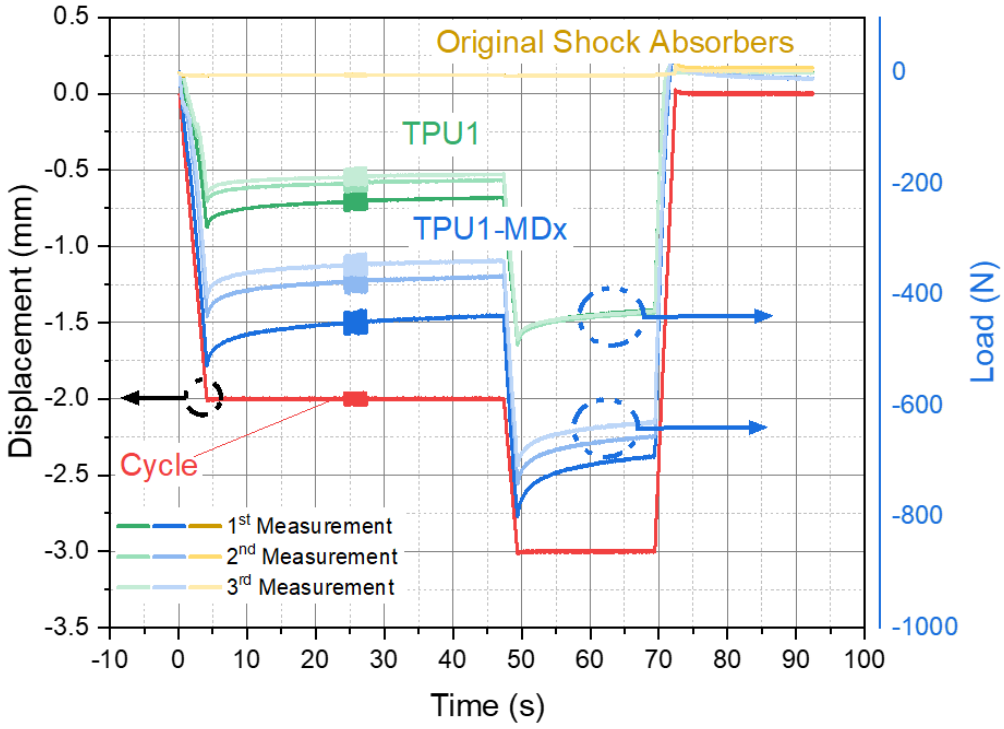

Figure 20: Load cycle of the TPUs and the original shock absorbers as well as the load curves of the analyzed TPU dampers.

highest rebound resilience values indicating lowest damping capacity (U_d/U_e). This is a particularly important insight for tailoring material properties with low stiffness and low damping capacity requirements.

Furthermore, a FEA model was set based on the material parameters determined from the hyperelastic characterizations. The model was validated by the simulation of a (rigid) ball drop onto an hyperelastic cylinder. Good agreement was found between the simulation and the performed rebound resilience experiments. This model can further be utilized to dimension (engineer) as well as optimize damping structures.

5. Conclusions

The applied methodology presents a systematic approach including data reduction as well as material parameter determination methods. The damping behavior is characterized sufficiently enough for product engineering and optimization of dampers with FE analyses. With that, classical shock absorbers can be redesigned with the utilization of material damping rather than structural damping. This, eventually, results in shock absorbers with reduced complexity, and components. In future research, the shock absorbers should be scaled to accommodate higher loads for better comparison to shock absorber characteristics carrying higher structural loads (self-weight). Additionally, the interface of the Fe particles and the TPU-matrix has to be analyzed in detail, even characterized within magnetic fields to exploit the magneto-active property changes.

Author Contributions: Conceptualization, U.D.C. and I.G.; methodology, U.D.C.; validation, U.D.C., C.E. and R.P.; formal analysis, C.E., R.P. and U.D.C; investigation, C.E. and R.P.; resources, U.D.C, I.G., Z.M.; data curation, C.E. and R.P.; writing—original draft preparation, U.D.C. and C.E.; writing—review and editing, U.D.C. and C.E.; visualization, U.D.C. and C.E.; supervision, U.D.C, I.G., Z.M.; project administration, U.D.C, I.G., Z.M.; funding acquisition, I.G. and U.D.C., All authors have read and agreed to the published version of the manuscript.

Funding: The financial support by the Austrian Federal Ministry for Digital and Economic Affairs, the National Foundation for Research, Technology and Development and the Christian Doppler Research Association is gratefully acknowledged.

Institutional Review Board Statement: Not applicable

Informed Consent Statement: Not applicable

Data Availability Statement: Not applicable

Acknowledgments: Open Access Funding by the Johannes Kepler University Linz is gratefully acknowledged. The support of Michael Lackner during the experimental work is highly appreciated.

Conflicts of Interest: The authors declare no conflict of interest

References

[1] G. Dong, D. Tessier and Y. F. Zhao, "Design of shoe soles using lattice structures fabricated by additive manufacturing.," *In Proceedings of the Design Society: International Conference on Engineering Design. Cambridge University Press.,* vol. Vol.1, no. No.1, pp. 719-728, 2019.

[2] U. D. Cakmak, F. HIptmaier and Z. Major, "Applicability of elastomer time-dependent behavior," in *Mech Time-Dependent Mater*, Springer Science+Business Media Dordrecht 2013, 2013.

[3] S. D., Dynamics and control for vibration isolation design. Ph.D. thesis, Virginia Polytechnic Institute and State University, 1997.

[4] Lamborghini, "lamborghini palm beach," Lamborghini, 6 11 2018. [Online]. Available: https://www.lamborghinipalmbeach.com/blog/what-is-a-lamborghini-active-suspension/. [Accessed 07 2021].

[5] M. Lokander and B. Stenberg, "Performance of isotropic magnetorheological rubber materials," *Polymeric Testing,* no. 22, pp. 245-251, 2003.

[6] F. J. Hiptmair, Z. Major, V. C. Barroso and S. Hild, "Experimental charcterization of magnetoelastomers and determination of material model parameters for simulations.," in *Proc. 10th Youth Symposium on Experimental Solid Mechanics (YSESM2011)*, Chemnitz, Germany, 2011.

[7] C. Niu, X. Dong and M. Qi, "Damping mechanism and theoretical model of electrorheological elastomers," *Soft Matter 13(32),* pp. 5409-5420, 2017.

[8] M. L. Auad, M. A. Mosiewicki, C. Uzunpinar and R. J. Wiliams, "Single-wall carbon nanotubes/epoxy elastomers exhibiting high damping capacity in an extended temperature range.," *Composites Science and Technology, 69(7-8),* pp. 1088-1092, 2009.

[9] J. Yang, X. Gong, H. Deng, L. Qin and S. Xuan, "Investigation on the mechanism of damping behavior of magnetorhelogical elastomers.," *Smart Materials and Structures, (21(12),* p. 125015.

[10] U. D. Cakmak and Z. Major, "Experimental thermomechanical analysis of elastomers under uni-and biaxial tensile stress state.," *Experimental Mechanics, 54(4),* pp. 653-663, 2014.

[11] T. Zehetbauer, A. Plöckinger, C. Emminger and U. D. Cakmak, "Mechanical design and performance analyses of a rubber-based peristaltic micro-dosing pump.," *Actuators. Multidisciplinary Digital Publisching Institute.,* vol. Vol.10, no. No.8, p. 198, 2021.

[12] U. D. Cakmak, I. Kallai and Z. Major, "Temperature dependent bulge test for elastomers.," *Mechanics Research Communications, 60,* pp. 27-32, 2014.

[13] F. Schneider, T. Fellner, J. Wilde and U. Wallrabe, "Mechanical proberties of silicones for MEMS.," *Journal of Micromechanics and Microengineering,* 2008.

[14] R. Moser, G. Kettlgruber, C. M. Siket, M. Drack, I. Graz, U. D. Cakmak, Z. Major, M. Kaltenbrunner and S. Bauer, "From Playroom to Lab: Tough Stretchable Electronics Analyzed with a Tabletop Tensile Tester Made from Toy-Bricks," 01 2016. [Online]. Available: https://onlinelibrary.wiley.com/doi/full/10.1002/advs.201500396. [Accessed 2021].

[15] M. Lindinger, "Traxxas BANDIT BLAU BUGGY RTR OHNE AKKU," [Online]. Available: https://www.lindinger.at/de/Fahrzeuge-Boote/Fahrzeug-Boots-Modelle/Offroad-4x4-Autos/Traxxas-BANDIT-BLAU-BUGGY-RTR-OHNE-AKKU-LADER-1-10-2WD-BUGGY-BRUSHED/9782245. [Accessed 07 2021].

[16] V. M. Miron, S. Lämmermann, U. D. Cakmak and Z. Major, "Material Characterization of 3D-printed Silicone Elastomers," *Structural Integrity Procedia, accepted,* 2021.

[17] N. W. Tschoegl, W. G. Knauss and I. Emri, "The effect of temperature and pressure on the mechanical properties of thermo-and/or piezorheologically simple polymeric materials in thermodynamic equilibrium-A critical review.," *Mechanics of Time-Dependent Materials, 6(1),* pp. 53-99, 2002.

[18] M. Liu and D. G. Gorman, "Formulation of Rayleigh damping and its extensions.," *Computers & Structures, 57(2),* pp. 277-285, 1995.